

A study of neural network-based evaluation methods for pipelines with multiple corrosive regions

Zhiwei Zhang^a, Songling Li^{a,*}, Huajie Wang^a, Hongliang Qian^a, Changqing Gong^a, Qiongyao Wu^b, Feng Fan^c

^a School of Ocean Engineering, Harbin Institute of Technology at Weihai, Weihai 264209, China

^b China Construction First Group Construction & Development Co., Ltd., Beijing 100102, China

^c School of Civil Engineering, Harbin Institute of Technology, Harbin 150000, China

ARTICLE INFO

Keywords:

Corroded pipeline
Remaining strength
Evaluation method
Digital images
Multiple corrosive regions
Neural networks

ABSTRACT

In recent years, significant developments have been made in methods for assessing the remaining strength of corroded pipelines. However, existing methods have limitations as they mainly focus on the local impact of corrosion defects. This study explores evaluation methods using neural networks to predict the ultimate resistance of pipelines containing multiple corrosive regions. Firstly, based on the validated method, the study generates a dataset comprising 3,000 corroded pipeline models and pixelates the corrosion information of these models via digital images. Then, three neural network evaluation frameworks are constructed: a Multilayer Perceptron (MLP) using the overall corrosion matrix, an MLP based on corrosion feature parameters, and Convolutional Neural Networks (CNN) based on corrosion images. Following this, the study analyzes the relationship between various corrosion parameters and failure pressure, compares the training effectiveness of the three neural network methods, and validates the accuracy and applicability of the proposed approach. The results indicated that various corrosion features should be considered when evaluating corroded pipelines, particularly depth. In addition, all three neural network-based methods show improved applicability and reliability compared to traditional evaluation methods, with CNN-image having the highest evaluation accuracy (correlation coefficient = 0.9564, average error = 3.46%).

1. Introduction

Since the 1960s, the global construction of oil and gas pipelines has developed rapidly, making the pipeline transportation industry a crucial hub for economic growth in various countries [1,2]. However, due to the complex environment and changing operational conditions, numerous significant incidents of pipeline failure and leakage have occurred worldwide [3,4]. Among these incidents, corrosion is the primary cause of pipeline failure [5,6]. Hence, given the high costs associated with repair or replacement, it becomes critically important to accurately evaluate the remaining strength of corroded pipelines to quantify the risk of failures and enhance safety levels in the design.

In recent years, extensive research has focused on evaluating corroded pipelines' remaining strength using traditional physical models. Initially, some standards and codes based on theoretical analysis and engineering practice have been established, such as ASME-B31G [7], Modified B31G [8], RSTRENG [9], CSA Z662-07 [10], PCORRC

[11], DNV-RP-F101 [12], and SY/T6151-2009 [13]. These standards primarily consider the influence of corrosion defects on pipeline strength and have been widely used in the industry. However, numerous studies have indicated limitations in using code standards to predict the ultimate load capacity [14,15]. Several modification methods have been proposed to address incomplete or oversimplified factors considered in these standards. Modifications have been made to the influence coefficients of various corrosion defect factors in the standards, such as width [16,17], length [18,19], and depth [20,21]. This approach primarily targets corroded pipelines with a single defect. The research becomes more complex for pipelines with interacting defects (Definitions of single and interacting defects are based on DNV-RP-F101 [12]). Some studies have investigated the limits and failure modes of interactions under various defect sizes and corrosion distributions [22–25]. Employing various theories, some researchers [26–29] have introduced methodologies for evaluating the remaining strength of pipelines containing multiple interacting corrosion defects.

* Corresponding author.

E-mail address: song575ling@163.com (S. Li).

Table 1
Basic parameters of the pipeline model.

Material	Yield strength (MPa)	Ultimate tensile strength (MPa)	L_0 (mm)	D (mm)	t (mm)	E (MPa)	ν
X80	556.3	697.6	2000	458.7	8.1	2×10^5	0.3

Furthermore, to address the research challenges posed by the complexity of corrosion shapes in practical scenarios, current studies have employed simplifications of these shapes. Consequently, some research has demonstrated the rationality of these simplifications [30, 31].

In recent years, due to its powerful computational capabilities in handling complex nonlinear problems, scholars have increasingly focused on ML methods [32, 33]. The three key elements of ML are data, models, and algorithms. Several studies have utilized various methods to generate large-scale corroded pipe data for ML applications, including FEM [34–38], modified empirical approaches [39], and hybrid empirical models [40, 41]. In addition, Adriano et al. [42] and Li et al. [43] applied discrete wavelet transform and locally linear embedding (LLE), respectively, for data preprocessing to extract corrosion features from high-dimensional nonlinear data. Hieu et al. [44] and Lu et al. [45] utilized various ML models to predict the burst pressure of corroded pipelines and evaluated the strengths and limitations of these models.

Due to the explosive growth of data and advancements in computational power, neural networks and deep learning have made significant breakthroughs in fields such as image recognition and natural language processing, becoming an important branch of ML. Initially, some studies combined neural networks with different algorithms to directly evaluate the failure pressure of corroded pipelines [46–51]. Ma et al. [52] and Yang et al. [53] proposed a failure evaluation mechanism based on the predictive results of neural networks. In addition, integrating neural networks with theoretical methods shows promising prospects. Chen et al. [54] optimized key empirical parameters in the Chen-Chu criteria [55] using neural networks, enhancing the accuracy of result predictions. Ma et al. [56] utilized prior knowledge from the Tresca criteria and the predictive capabilities of ensemble learning to propose a novel hybrid approximation model for predicting the burst pressure of corroded pipelines.

However, the current research still has some limitations. Existing evaluation methods primarily focus on the corrosion effects in localized areas of pipelines, such as a single defect or several defects within limited zones. However, in actual pipelines, corrosion typically manifests in a dispersed and stochastic manner across the entire circumferential area of the pipe [57–60], complicating the information landscape. Traditional physics-based approaches often rely on manually extracted corrosion features and use approximated simplifications in evaluation methods, potentially increasing uncertainties in structural reliability, which contradicts the current pursuit of precise system safety. Alternatively, the introduction of neural network methods provides potential solutions to this issue by enabling simultaneous handling of more feature information and addressing highly nonlinear problems. However, applying neural network methods requires robust support from a reliable dataset. Although full-scale experiments can provide relatively dependable partial data, their high costs restrict the availability of sufficient data. Hence, an efficient numerical simulation method is a preferable alternative [34–38].

Accordingly, this study focuses on the remaining strength of pipelines with multiple corrosive defects using neural networks. Initially, the study generates a dataset with 3,000 samples of validated corroded pipe models and pixelates the corrosion information of these models using digital images. Then, this study develops three neural network evaluation frameworks: MLP based on the overall corrosion matrix, MLP based on corrosion feature parameters, and CNN based on corrosion images. Finally, this study compares the computational results of various methods using experimental samples with localized corrosion and test samples with multi-corrosion regions.

2. Establishment of the dataset

2.1. Validation of the finite element method (FEM)

The model is established based on the pipeline samples from the experiment [61], and the basic parameters of the pipe model are listed in Table 1, where D is the diameter, t is the wall thickness, L_0 is the length of the pipeline, E is the elastic modulus, and ν is the Poisson's ratio. In addition, some experimental studies have indicated that the Ramberg-Osgood constitutive model [62] can simulate the nonlinear characteristics of high-strength steels [63–65]. The mesh division and boundary condition of the model are illustrated in Fig. 1. Internal

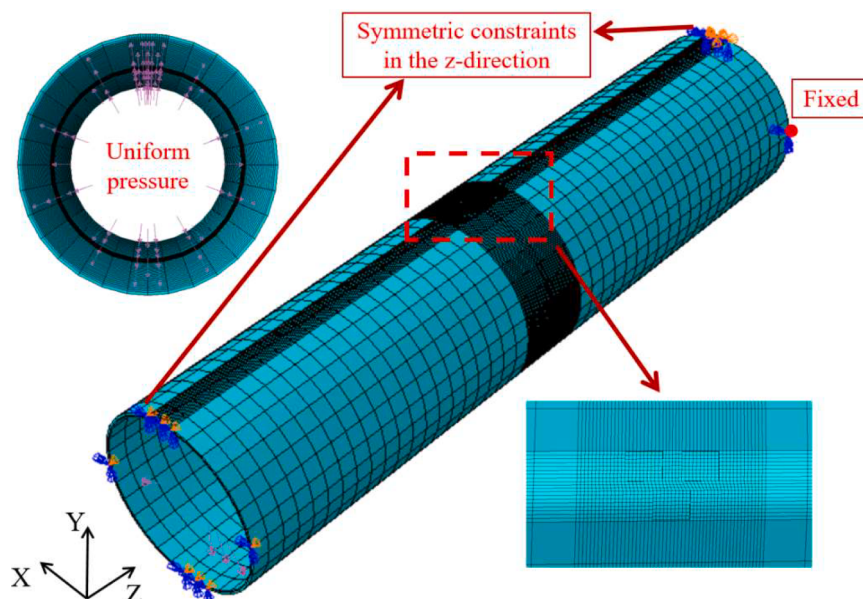
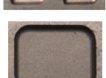


Fig. 1. Mesh division and boundary condition of pipe model.

Table 2

Comparison of failure pressure in experiment and FEM.

Specimen	Diagram	Experiment (MPa)	FEM (MPa)	Error (%)
IDTS 2		22.68	21.70	4.01
IDTS 3		20.31	20.28	0.15
IDTS 4		21.14	21.44	1.42
IDTS 5		20.87	21.11	1.15
IDTS 6		18.66	18.81	0.80
IDTS 7		18.77	19.2	2.31
IDTS 8		24.20	24.36	0.66
IDTS 9		23.06	24.19	4.90
IDTS 10		23.23	23.53	1.29
IDTS 11		21.26	21.56	1.41
IDTS 12		20.16	20.355	0.97

pressure remains the predominant load parameter for pipelines [66–69]. Therefore, uniform pressure is applied to the inner surface of the model. Regarding elements, the model utilizes the linear brick element named C3D8R, an 8-node solid element in ABAQUS with reduced integration (1 integration point) and hourglass control. The plastic failure criterion is adopted due to the strain hardening of the steel material. It is considered that failure occurs when the minimum von Mises stress at the corroded zone ligament equals the ultimate tensile strength of the steel pipe [70, 71].

Table 2 and Fig. 2 compare between the failure pressure and failure modes of the experimental results and FEM, respectively. The results indicate that an average error between the predicted and measured values is approximately 1.74%. In addition, the failure mode of the model aligns with the observed failure behavior in the experiments, confirming the effectiveness and accuracy of the FEM.

2.2. Model of pipes with multiple corrosive regions

2.2.1. Pixelization of corrosion information via digital images

Before creating the dataset, it is necessary to identify a method that can effectively extract and express the corrosion information. Similar to digital images, this study employs the concept of image pixels to segment the corrosion morphology. The schematic diagram for

extracting corrosion information using digital images is shown in Fig. 3. Each digital image consists of a pixel matrix, where the geometric dimensions of the pixels represent the axial length and circumferential angle of the pipeline, and the pixel values represent the corrosion depth ratio d/t .

2.2.2. Dimension analysis of pixel point size

In digital images, pixel size significantly impacts image resolution. Similarly, various pixel sizes affect the range of extractable corrosion information. On the one hand, substantial pixel sizes can result in the loss of corrosion information (Fig. 4). The range of corrosion information represented by the corrosion matrix can lack representativeness. On the other hand, smaller pixel sizes provide a more accurate description of corrosion morphology with reduced error but at the expense of increased computational resources. In addition, to ensure the mesh coherence of the model, this study defines the mesh size of the pipe model by pixel size, which also affects the results of FEM. Hence, choosing an appropriate pixel size is necessary.

This study compares the simulation results of three experimental samples (IDTS 3, IDTS 5, and IDTS 7) under different pixel sizes. A combination of integer division, remainder, and rounding is employed to merge pixels for corrosion defect sizes that do not satisfy integer multiples of the pixel size. During the process of developing the pipe

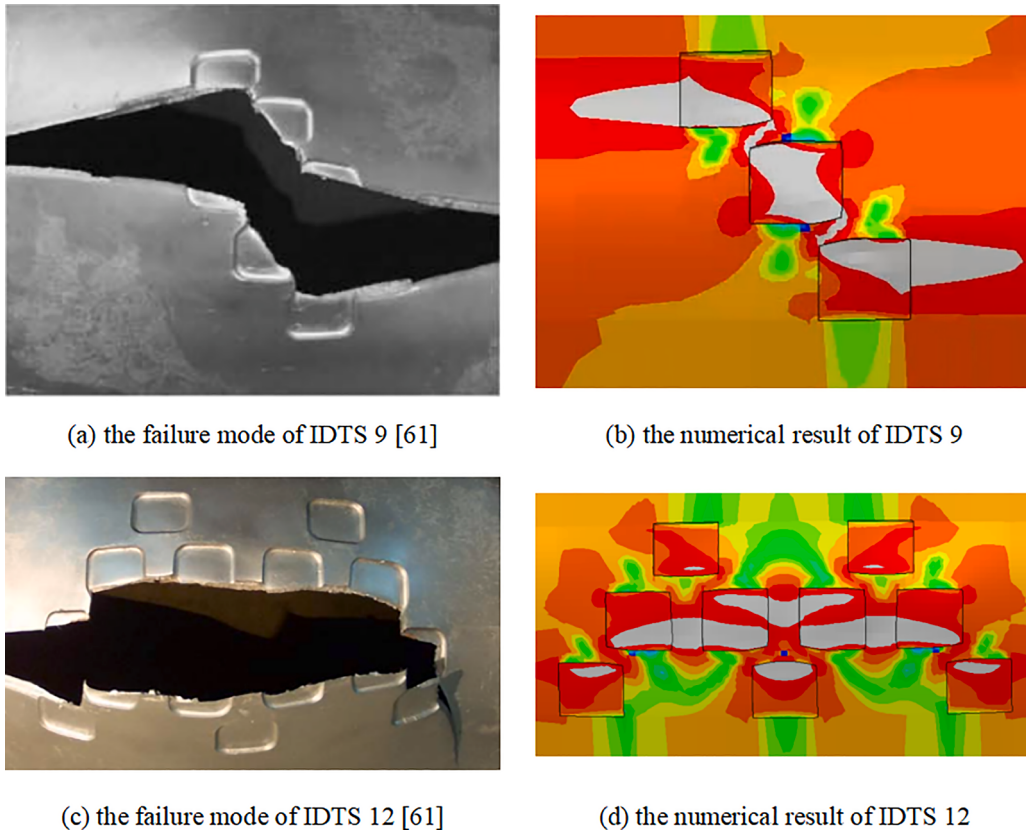


Fig. 2. Comparisons of failure mode in experiment and FEM.

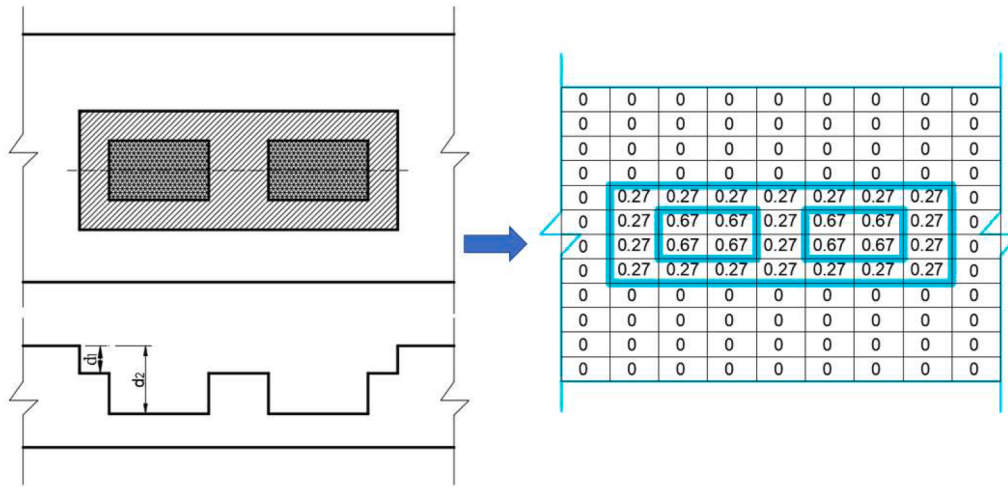


Fig. 3. Extract corrosion information via digital image.

model, the mesh size of the model is determined by pixel points, establishing a direct relationship between mesh size and pixel size. Fig. 5 illustrates the segmentation method of IDTS 3 under different pixel sizes.

The results of FEM for the three samples under various pixel size divisions are depicted in Tables 3, 4, and Fig. 6. On the one hand, the increase in pixel length causes a larger error. This phenomenon is likely due to the errors introduced using excessively large pixels to describe the actual corrosion morphology. On the other hand, the impact of pixel width on the results is insignificant, which corroborates the conclusions of some previous studies [28–31]: the effect of corrosion width on strength is negligible at small scales.

The final pixel size is set to 5 mm × 4°. At this size, the overall

deviation exhibits a smaller range of variation, indicating that the simplification of the analysis for large corrosion regions is acceptable.

2.2.3. Modeling method for pipelines with multiple corrosion regions

Li [30] and Mojtaba [31] have demonstrated the rationality of using a rectangular shape to simplify corrosion shapes when the corrosion volume ratio is close. As a result, this study utilizes PYTHON to develop a pipe model with multiple rectangular corrosive regions in ABAQUS. The overall process is illustrated in Fig. 7. Specifically, the pixel size is set to 5 mm × 4°, representing the axial length and the circumferential width of corrosion. In addition, the pixel values indicate the depth ratio of the corrosion defect, d/t ranging from 0 to 1. A numerical matrix of

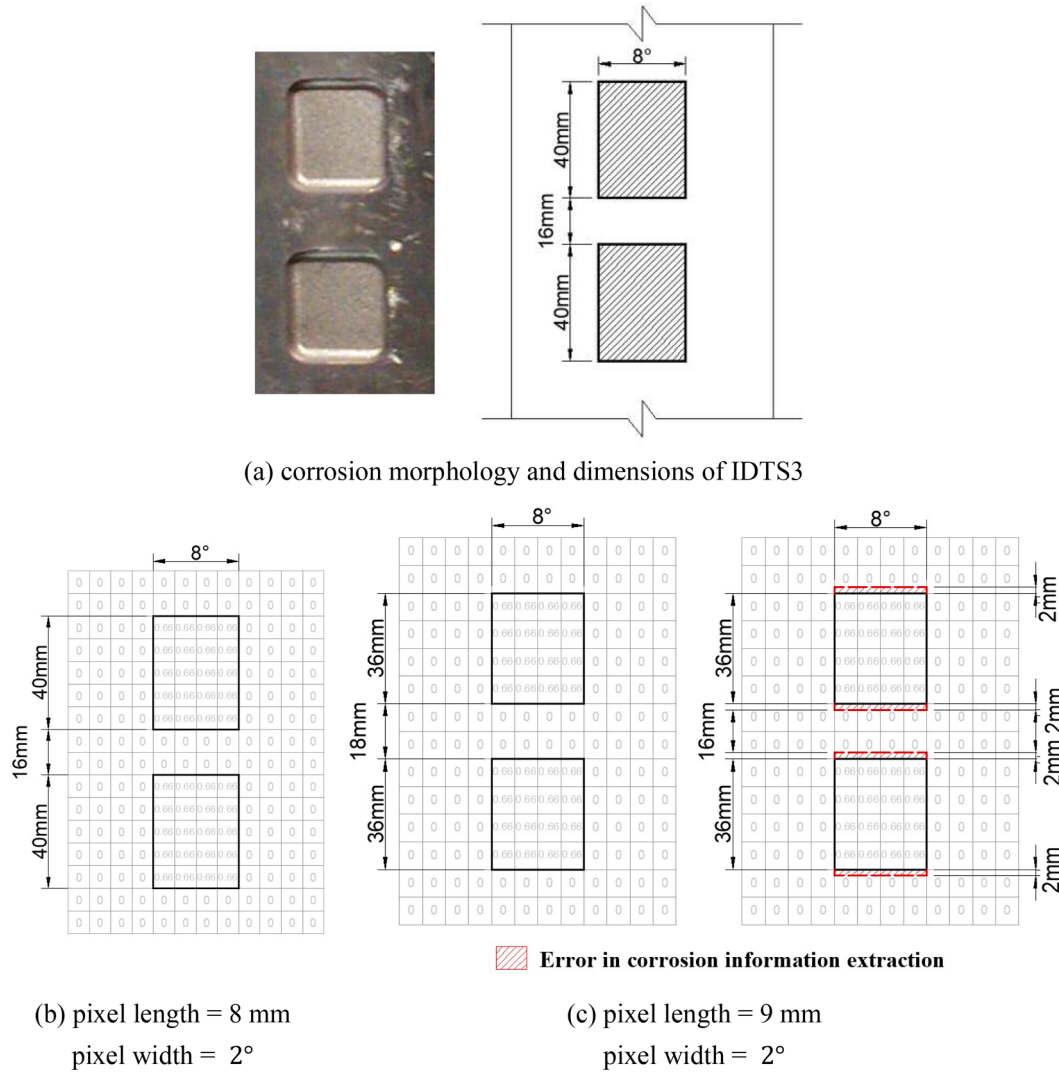


Fig. 4. The corrosion image matrix of the IDTS3 with different pixel sizes.

90×90 is adopted to simulate the corrosion situation in the entire pipe section. The process unfolds as follows:

- (1) Based on the previously mentioned validation of the FEM, this study creates an intact pipeline model incorporating geometric and material parameters detailed in Table 1.
- (2) Generate instances with random corrosion defects:
 - a) Different analysis groups are set up, and a specified number of rectangular blocks k are assigned to each group.
 - b) The size and position parameters of each corrosion block are determined through random generation. These parameters include the length, width, and depth of the corrosion block, where the length and width correspond to the number of pixels in the axial and circumferential directions, respectively, and the depth corresponds to the pixel values within the corrosion block.
 - c) The Move and Rotate methods in the Assemble module are employed to position the corrosion pits. Then, the Boolean Operation is employed to etch the surface of the pipeline, generating an instance with random pits. The pipe model with random pitting corrosion is depicted in Fig. 8.
 - d) The corrosion blocks are assembled into the specified region to create the overall corrosion matrix. This matrix represents the digital image that has extracted corrosion information.

(3) Boundary conditions and loads are applied to the model, and the mesh is delimited to finalize the model.

The pipeline model with multiple corrosion areas established in this study more closely aligns with the actual corrosion morphology observed. However, developing such a pipeline model using FEM through traditional manual spatial Boolean operations often results in a substantial workload, with modeling times typically ranging from 5 to 10 h. In contrast, using the overall matrix and PYTHON can significantly enhance modeling efficiency. The proposed method in this study requires only 10–20 min, achieving a time reduction of approximately 30-fold.

2.3. Creation and distribution of the dataset

Pluvinage et al. [72] and Shuai et al. [73] conducted statistical analyses of corrosion detection data from active pipelines in Algeria and Chinese maritime regions, respectively. The statistical results indicated strong randomness in the occurrence of pipeline corrosion defects, with significant variability in distribution parameters observed under different environmental conditions. However, both investigations determined that corrosion defects are uniformly distributed along the circumferential regions of the pipelines and exhibit no correlation. Hence, the pipe models with multiple corrosive regions in this study are

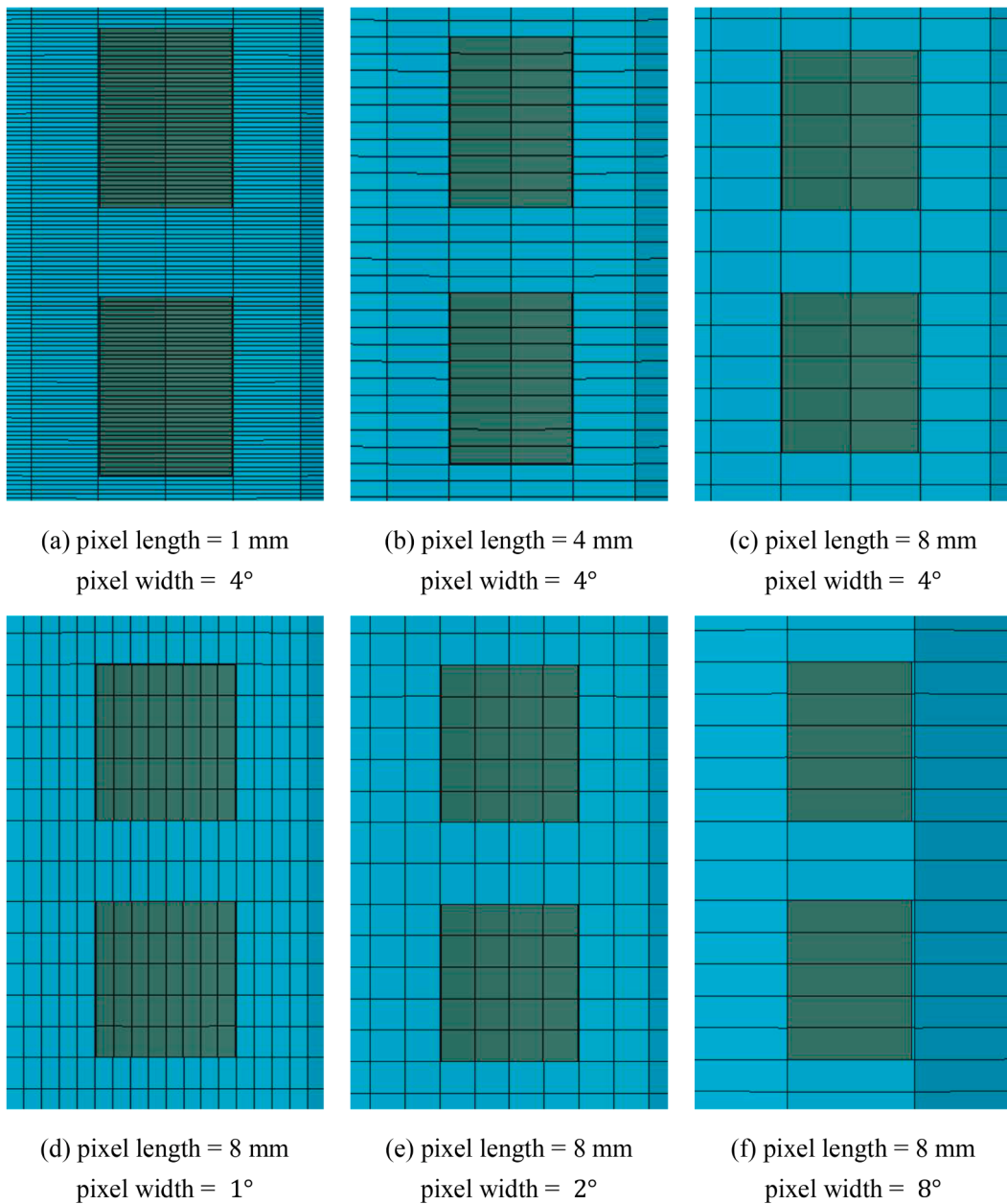


Fig. 5. Model of the IDTS3 with different pixel sizes.

Table 3
FEM error at different pixel lengths (%).

Specimen	Length of pixel point (mm)							
	1	2	3	4	5	6	7	8
IDTS 3	0.622	0.111	0.625	0.464	0.397	0.181	0.489	0.013
IDTS 5	0.833	0.921	0.474	0.701	0.728	2.926	1.963	2.443
IDTS 7	1.003	0.734	1.219	1.249	1.287	2.245	4.149	3.777
Average	0.820	0.589	0.773	0.805	0.804	1.784	2.200	2.078

more accurately consistent with the actual corrosion morphology. Based on the statistical data and the modeling above method, this study has generated a dataset comprising 3,000 samples. The distribution of method parameters is detailed in Table 5, and the statistical distribution plot of the dataset parameters is illustrated in Fig. 9.

The parameter (k), representing the number of defects, is estimated using the defect density per unit length of pipelines in service [72]. The

defects' geometric parameters primarily derive from statistical data. In addition, the pipeline's structural integrity is compromised when the defect depth ratio reaches 70% to 80%, based on some standards [10, 13]. Therefore, the maximum and minimum depths of the defects are limited. In the dataset samples, the fundamental parameters of defect distribution also agree with the results of an extreme value normal distribution analyzed in the statistical survey [72,73].

Table 4

FEM error at different pixel widths (%).

Specimen	Width of pixel point (°)							
	1	2	3	4	5	6	7	8
IDTS 3	1.176	1.142	1.407	1.199	1.429	1.583	1.331	1.488
IDTS 5	2.374	2.165	2.527	2.156	2.245	2.333	2.589	2.363
IDTS 7	2.352	2.445	2.378	2.333	2.346	2.635	2.567	2.557
Average	1.967	1.917	2.104	1.896	2.006	2.184	2.162	2.136

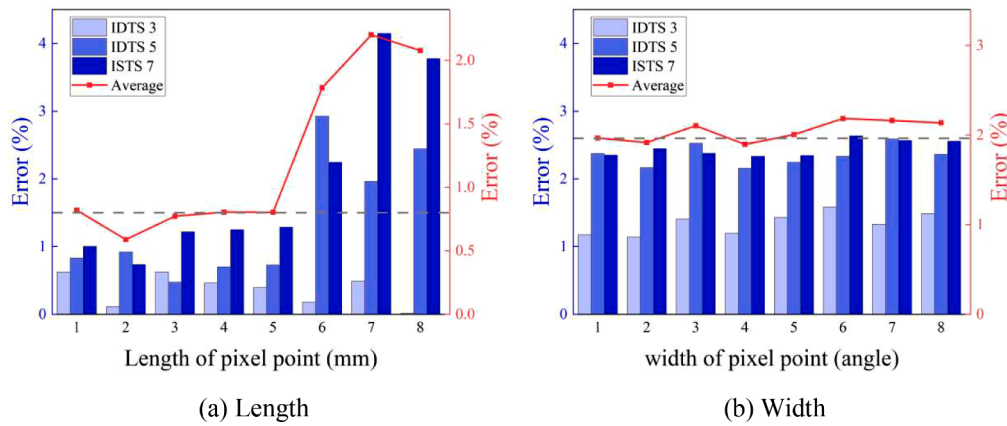


Fig. 6. Results at different lengths and widths of pixel points.

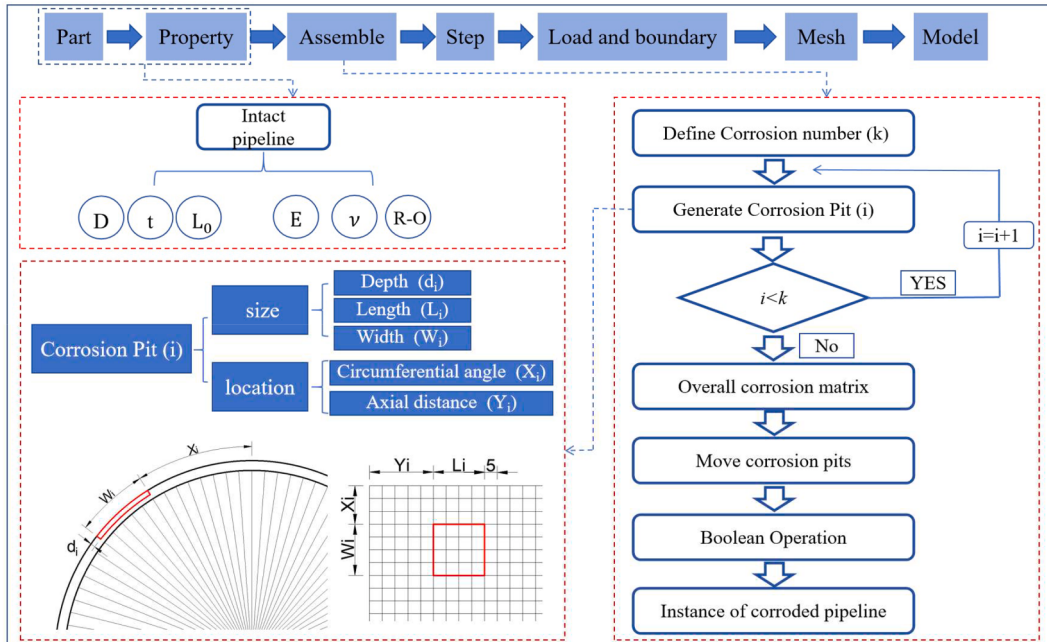


Fig. 7. Framework to establish the model with multiple corrosion regions.

Several widely used neural network methods currently exist, including Feedforward Neural Networks (FNNs), Convolutional Neural Networks, Recurrent Neural Networks (RNNs), Generative Adversarial Networks (GANs), and Deep Belief Networks (DBNs), suited to various data structures and problem frameworks. This study selects MLP and CNN as the fundamental model frameworks because the evaluation method for the remaining strength of corroded pipelines is essentially a regression problem. MLP, as a foundational deep learning algorithm, demonstrates flexibility in handling datasets characterized by complex features and high randomness. In contrast, CNN excels with digital

image datasets, effectively capturing spatial structural features and extracting critical information from corrosion images.

3. Evaluation method of MLP

3.1. Preliminary

The basic working mechanism of a single-layer, single-neuron network structure model is illustrated in Fig. 10(a), where the weights w is the connections between each pair of neurons from the input layer to

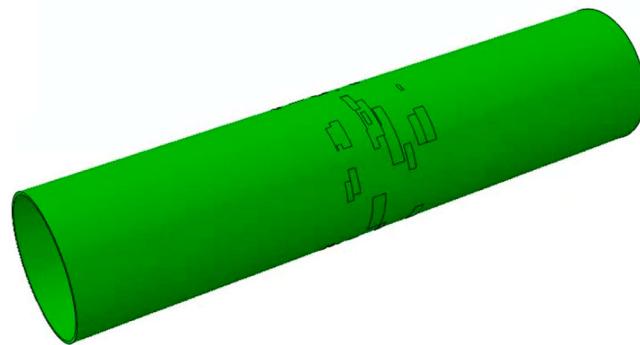


Fig. 8. Pipe model with multiple corrosive regions.

Table 5
Distribution of random variables in the model.

	Parameters	Distribution type	Note
Number of defects	k	Uniform	Range: [20, 35]
Geometric parameters of defects	d (mm)	Normal	Mean: 4; Max: 6.075; Min: 0.81
	L (mm)	Lognormal	Mean: [80, 120]; std: 50
	W (mm)	Lognormal	Mean: [60,100]; std: 60
Positional parameters of defects	X (mm)	Uniform	Range: [0, 450]; interval: 5
	Y (°)	Uniform	Range: [0,360]; interval: 4

the hidden layer, while the biases b correspond to each neuron, and the activation function f is applied to the weighted sum of inputs plus the bias to produce the output. Thus, the loss function value is derived by comparing the output with the original data. A new output is obtained utilizing the gradient descent method to update the weights and biases based on the loss function. Hence, this iterative process gradually reduces the loss until the desired level of accuracy is achieved.

The capacity of a single neuron or network layer to address problems is inherently limited, leading to the development of the Multilayer Perceptron (MLP). This model structure within deep learning is characterized primarily by including multiple neurons in the hidden layers (Fig. 10(b)), which offers a more precise solution for complex, high-order nonlinear problems.

3.2. The evaluation method of MLP based on the overall matrix (MLP-matrix)

The neural network model is established with 90×90 inputs obtained by flattening the overall matrix and using the failure pressure as the output (Fig. 11). Data normalization preprocessing occurs before model training, and the Mean Squared Error (MSE) is selected as the loss function. Among the 3,000 samples in the dataset, 2400 are allocated for training, while the remaining 600 are retained for testing.

Neural networks represent a practical science; for various problems and network structures, continuous adjustment of model parameters is necessary to achieve optimal results. Fig. 12 depicts the training outcomes of the network under different activation functions, learning rates, batch sizes, and optimizers. The results indicate that a larger learning rate leads to faster iteration speed but slightly inferior convergence results. In addition, increasing the batch size reduces training time but requires substantial computational resources. During training, phenomena of gradient dispersion and unstable oscillations in calculation results occur. Different optimizers and activation functions also impact the iteration speed and results. Based on the iteration

performance of each parameter, the parameter combination that yielded the best training results was selected. Table 6 provides the final parameters of the MLP-matrix.

Overfitting is a common issue in neural networks, where the model excessively fits noise and outliers in the training data, leading to good performance on the training data but poor performance on the testing data. This study addresses this issue using two regularization techniques: Dropout [74] and L2 regularization [75]. The dropout method reduces dependencies between neurons by randomly dropping some neurons in each training batch, as illustrated in Fig. 13. L2 regularization penalizes large weight values by adding a regularization term based on the sum of the weight parameters squared to the loss function. This promotes a more uniform weight distribution and a simpler model. Based on the training results, regularization has enhanced the comparability between the training and test sets, improving the robustness of complex neural network models.

3.3. The evaluation method of MLP based on corrosion feature (MLP-feature)

Using the complete overall matrix as the input for the neural network, without the step of corrosion feature extraction, increased the difficulty of network training and indirectly decreased the training effectiveness. Hence, drawing from other studies [46–48], this research extracts seven corrosion features from the matrix to address this issue. The corrosion parameters include the maximum depth of the defect d_{\max} , the maximum length of the defect L_{\max} , the maximum width of the defect W_{\max} , corrosion volume V , corrosion area S , 50th percentile depth of the defect d_{50} , and 75th percentile depth of the defect d_{75} . Table 7 lists the optimized parameters of the MLP evaluation method based on these corrosion features, while the network model structure and training process are illustrated in Fig. 14.

Figs. 15 and 16 depict the Pearson correlation matrix among the various parameters and the neural network training process under specific corrosion feature combinations, aiming to elucidate the relationship between the corrosion features and the failure pressure in more detail. In Fig. 16, Combination 0 represents the complete set of seven corrosion features; Combination 1 includes the radial profile information of the pipeline, comprising d_{\max} , d_{mean} , d_{75} , and d_{50} ; Combination 2 encompasses the axial surface information of the pipeline, including L_{\max} , W_{\max} , and S ; and Combination 3 depicts a composite of significant corrosion feature information, including d_{\max} , L_{\max} , and W_{\max} .

The parameters associated with defect depth (d_{\max} , d_{mean} , d_{75} , d_{50}) are the most critical factors influencing the result. Compared to other features, the parameters associated with defect depth exhibit significantly larger correlation coefficients with the failure pressure. In addition, the training process of the neural network validates this conclusion, as a significant decrease in training effectiveness occurs when only considering the axial surface information of the corroded pipeline and neglecting the radial profile information.

It is essential to comprehensively consider multiple corrosion features to evaluate the remaining strength of corroded pipelines. A single factor cannot exhibit a very strong correlation with the result (all correlations are less than 0.8), making it difficult to decisively impact the results. In addition, the training performance using a composite of features is superior to solely profile feature information. Accordingly, the training results are most stable when using the seven corrosion features.

4. Evaluation method of CNN based on corrosion image (CNN-image)

4.1. Basic structure of convolutional neural networks

The CNN is a deep learning model widely used in the field of computer vision. It excels in tasks such as image recognition, object detection, and image segmentation. Its unique advantage lies in its ability to

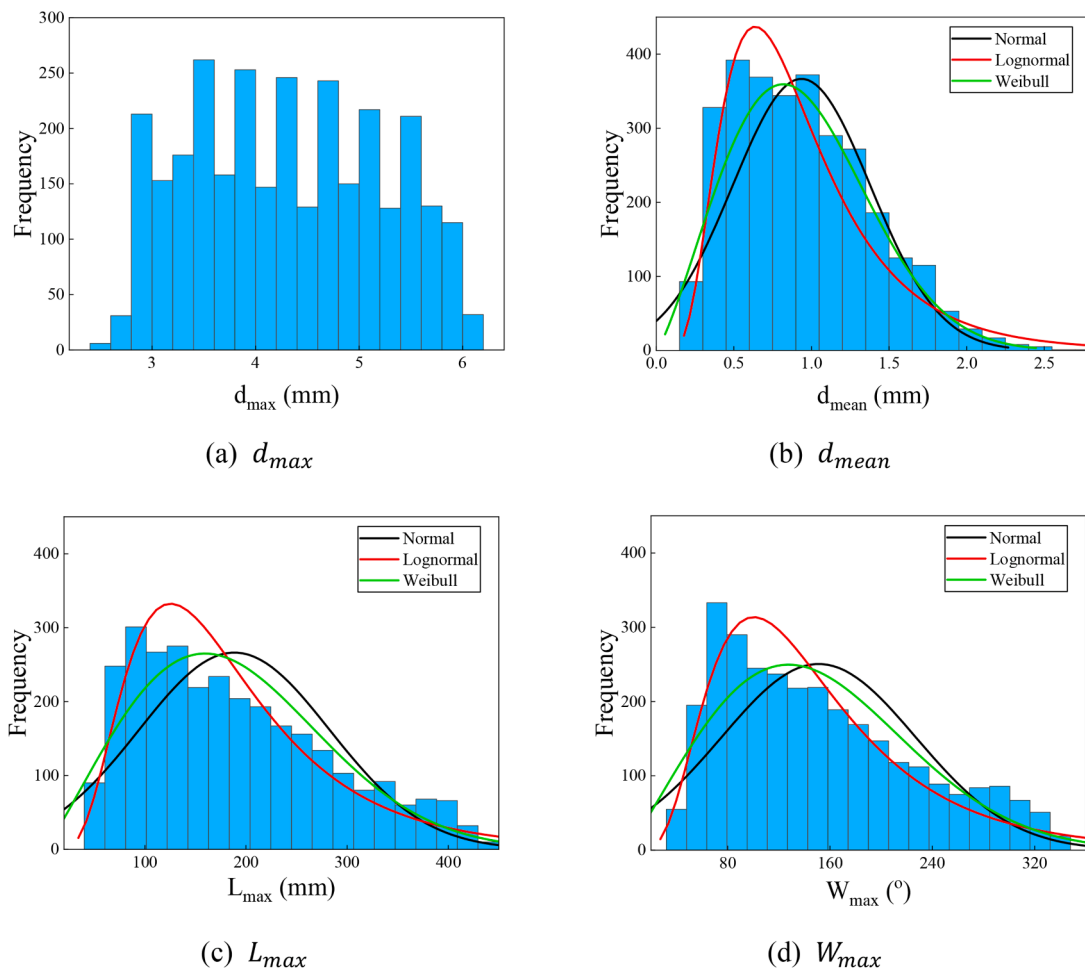


Fig. 9. Statistical distribution of parameters in the dataset.

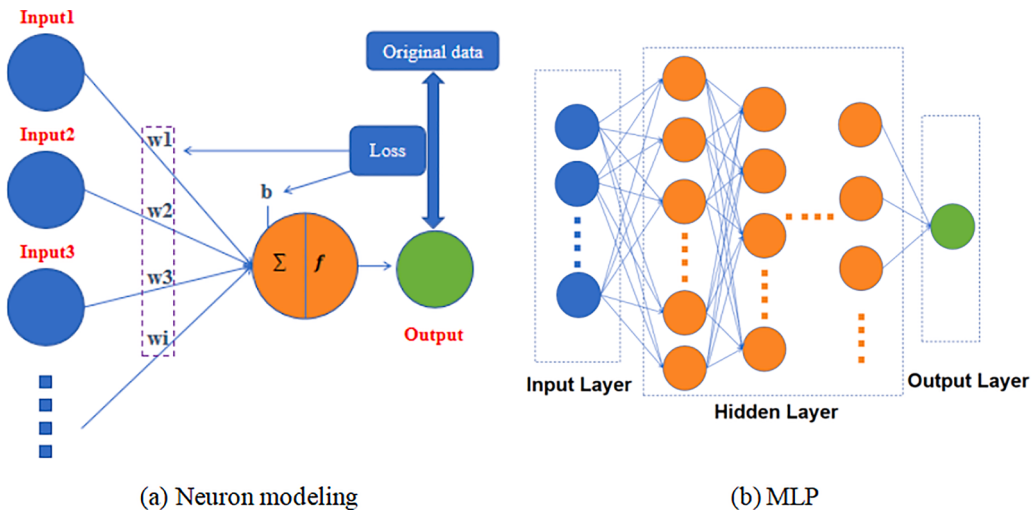


Fig. 10. Basic structure of a single neuron and the MLP.

gradually extract higher-level and more abstract features through multiple layers of convolution and pooling operations. CNN exhibits properties such as translation invariance and partial position invariance, which contribute to its effectiveness in analyzing visual data.

CNN represents a hierarchical neural network structure that combines convolutional, pooling, and fully connected layers. In the convolution operation, a filter (convolutional kernel) slides over the input data

to compute the element-wise product within a local region, summing the results to generate a feature map. Multiple filters are employed to extract distinct features. Pooling operations reduce the spatial dimensions and parameter count of the feature maps, decreasing computational complexity. Common pooling methods include max pooling and average pooling [76], with this study opting for max pooling in the pooling layer to retain the most prominent features in the image. The

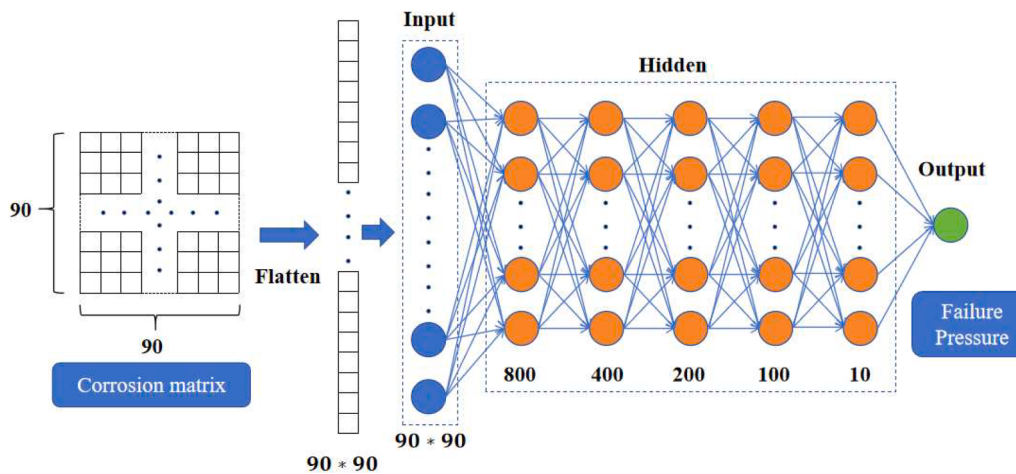


Fig. 11. Network structure of MLP-matrix.

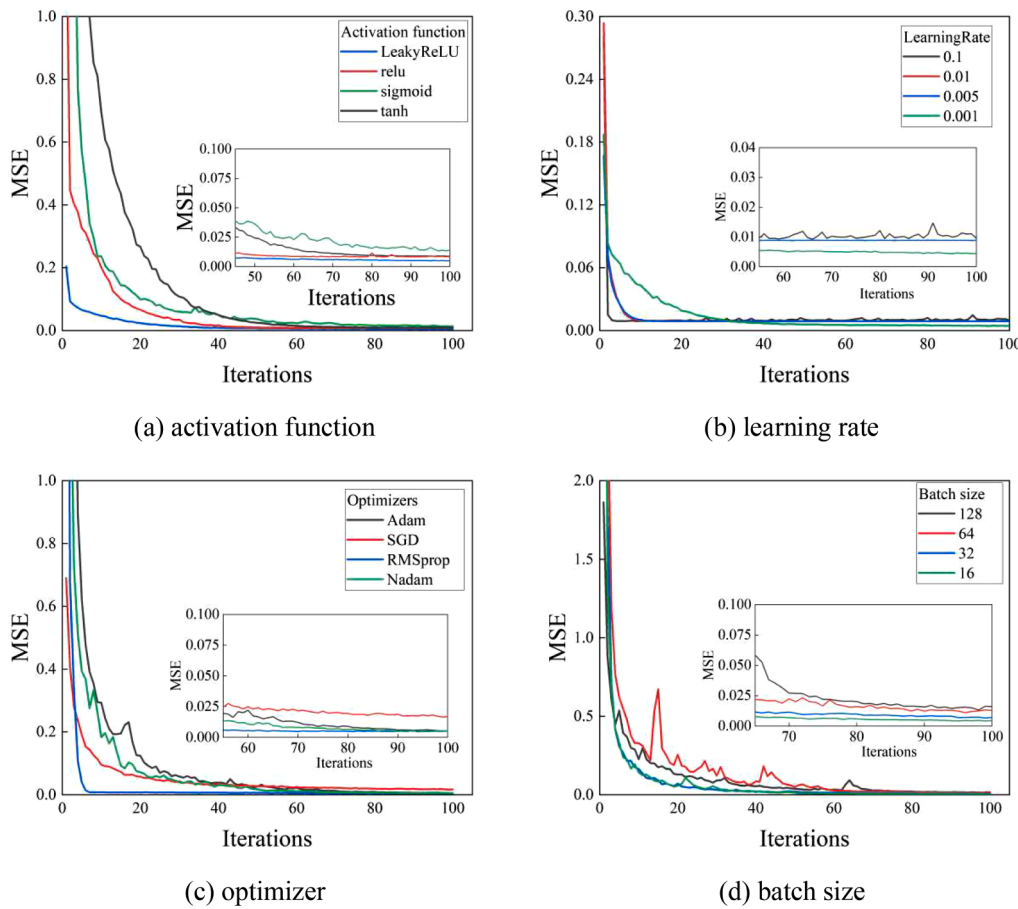


Fig. 12. Training process with different neural network parameters.

Table 6
The final parameters of MLP-matrix.

Parameters	Value
The architecture of the neural network	8100-800-400-200-100-10-1
Batch size	16
Loss function	Mean squared error
Activation function	LeakyReLU
Optimizer	Adaptive Moment Estimation (learning rate=0.001)

process of convolution and pooling is illustrated in Fig. 17.

4.2. Data augmentation

This study utilized the method of Data Augmentation to expand the original dataset and address the substantial data requirements of CNN. As an essential approach in deep learning, Data Augmentation generates new training samples by applying a series of random transformations and expansions to the original data, increasing the diversity and quantity of the data and improving the model's generalization ability and robustness. Given the translation and partial position invariance of

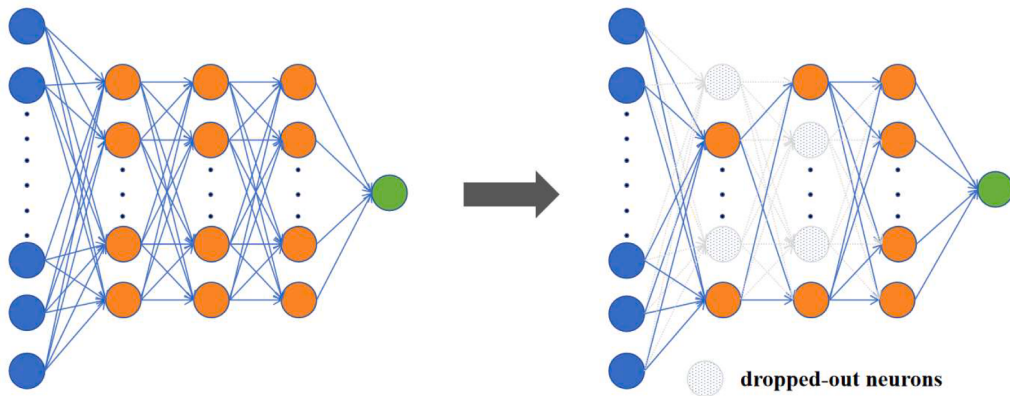


Fig. 13. Dropout method.

Table 7
Final parameters of the MLP-feature.

Parameters	Value
The architecture of the neural network	7-32-16-8-1
Batch size	16
Loss function	Mean squared error
Activation function	LeakyReLU
Optimizer	Adaptive Moment Estimation (learning rate=0.001)
Dropout rate	0.4
Regularization coefficient	0.001

CNNs, this study employs two methods, Random Flip and Random Crop (Fig. 18), to augment the original 2400 training samples to 7200.

4.3. The training process of CNN

This study customizes a CNN structure based on the convolutional block architecture of VGG-16 [77], as illustrated in Fig. 19.

The training process of the model under different combinations of kernel size, pool size, number of convolution blocks, and number of dense layers is depicted in Fig. 20. The training effectiveness of the CNN improves with an increase in the number of convolution blocks, largely due to the more efficient extraction of essential features by multiple convolution blocks. The impact of kernel size, pool size, and dense number on MSE is not particularly pronounced. However, smaller or

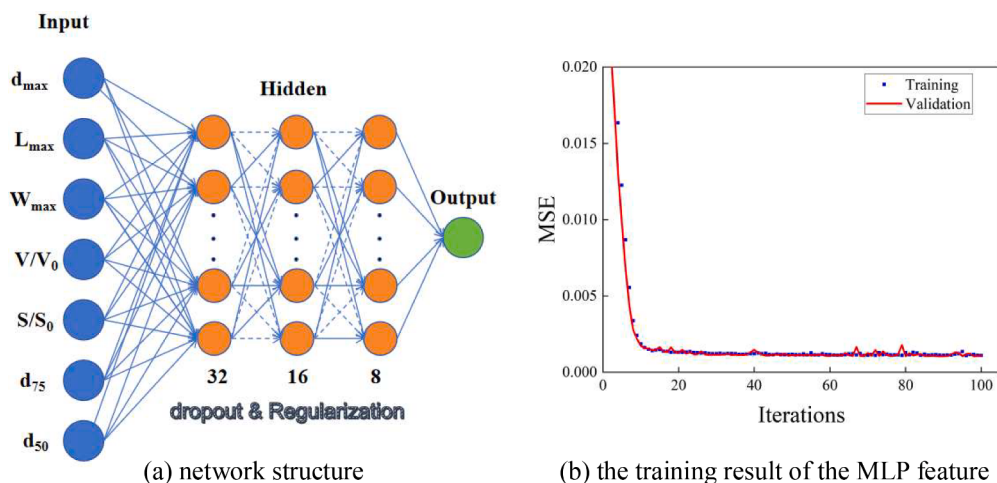


Fig. 14. Network structure and training result of the MLP feature.

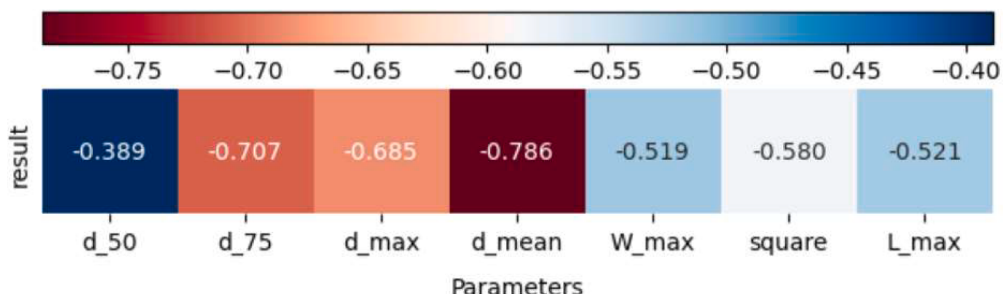


Fig. 15. Pearson correlation matrix between remaining strength and corrosion features.

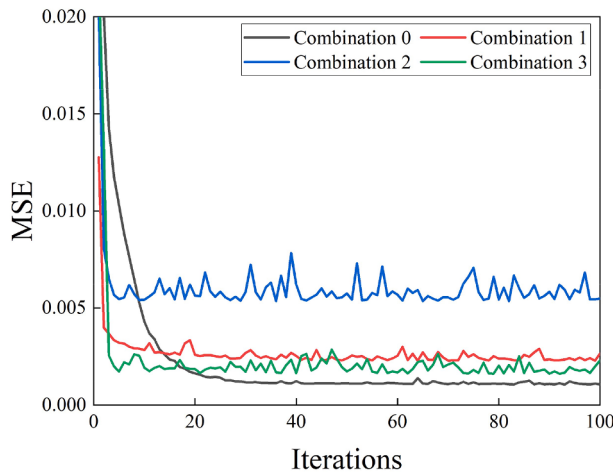


Fig. 16. Training process under specific corrosion feature combinations.

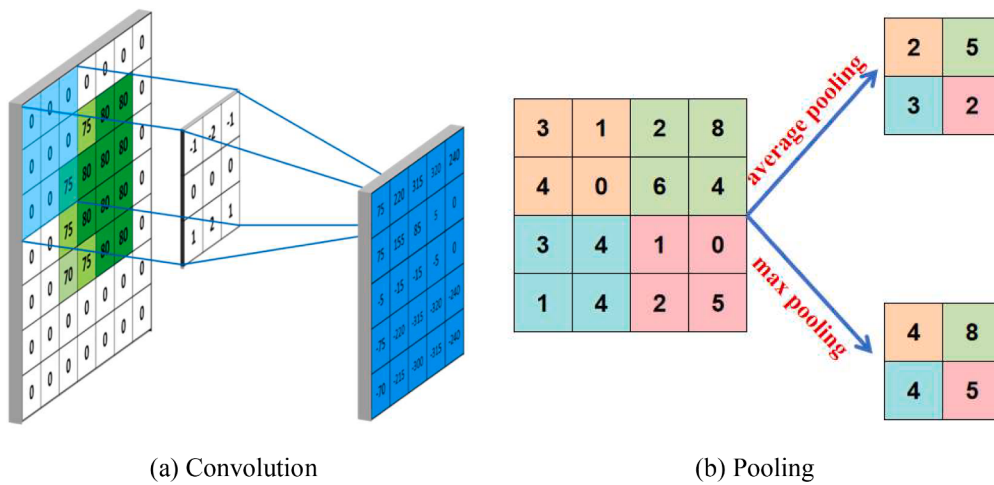


Fig. 17. Operations in convolutional neural networks.

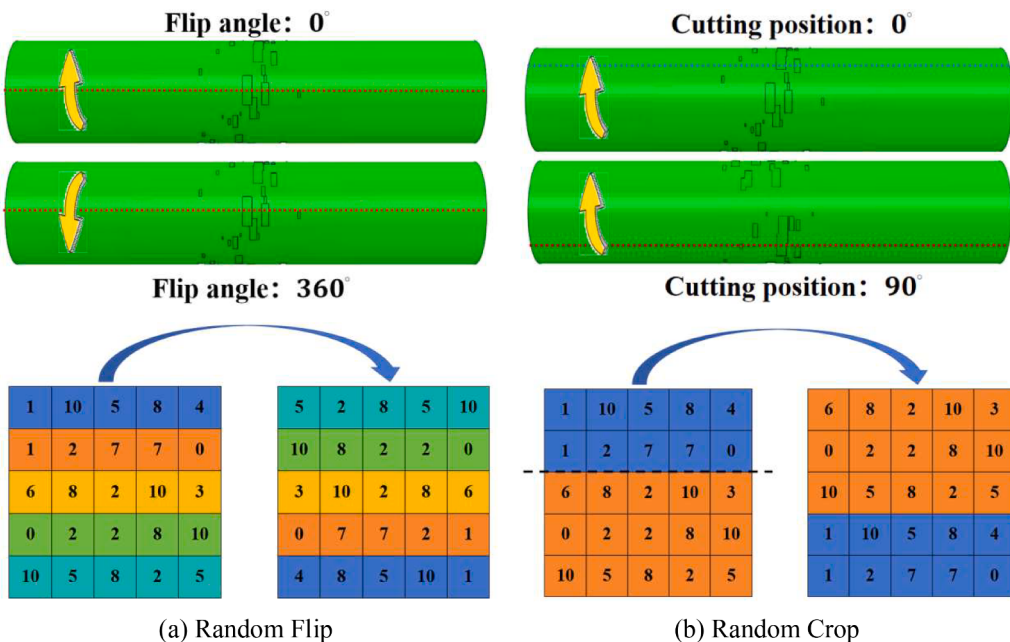


Fig. 18. Illustration of the data augmentation method.

larger values tend to yield a more stable convergence. The structural parameters of the convolutional and fully connected layers in the CNN are presented in Table 8. The final training results are shown in Fig. 21.

5. Results comparison and validation

5.1. Comparison of neural network methods

The prediction results of three different neural network models on a test dataset of 200 samples are depicted in Fig. 22. Overall, MLP-feature surpasses MLP-matrix, while CNN-image exhibits the best performance. Under the CNN-image method, the average error is only 3.46%, and the correlation coefficient between predicted and actual values reaches 0.9546.

On the one hand, compared to MLP-matrix, the MLP-feature method extracts features from the corrosion information, reducing the prediction task for neural networks and improving computational efficiency. On the other hand, the CNN-image method gradually learns abstract features of the corrosion image by layering multiple convolutional and

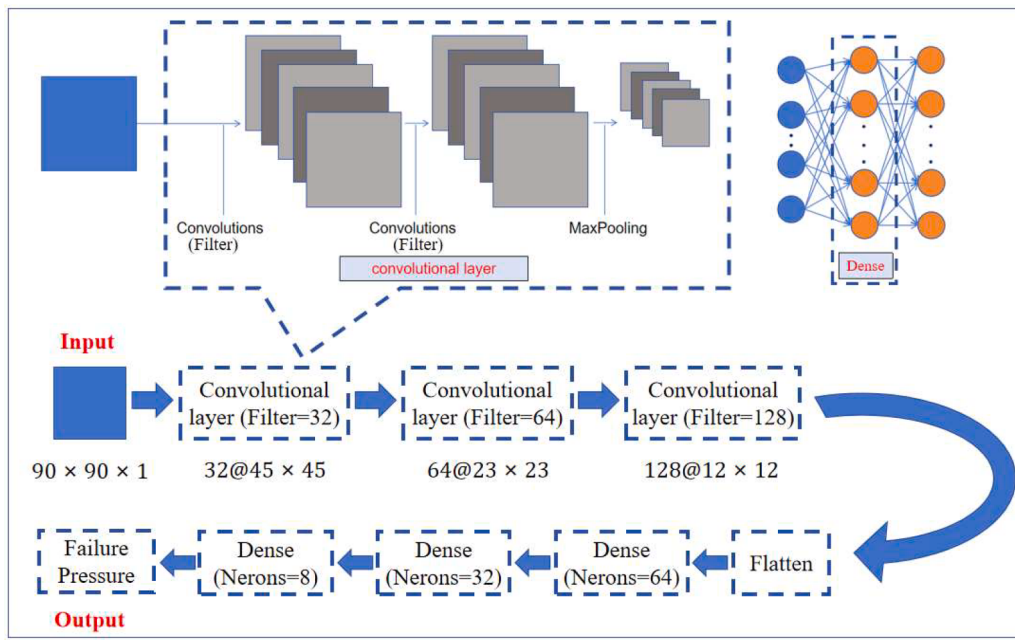


Fig. 19. Network structure of CNN-image.

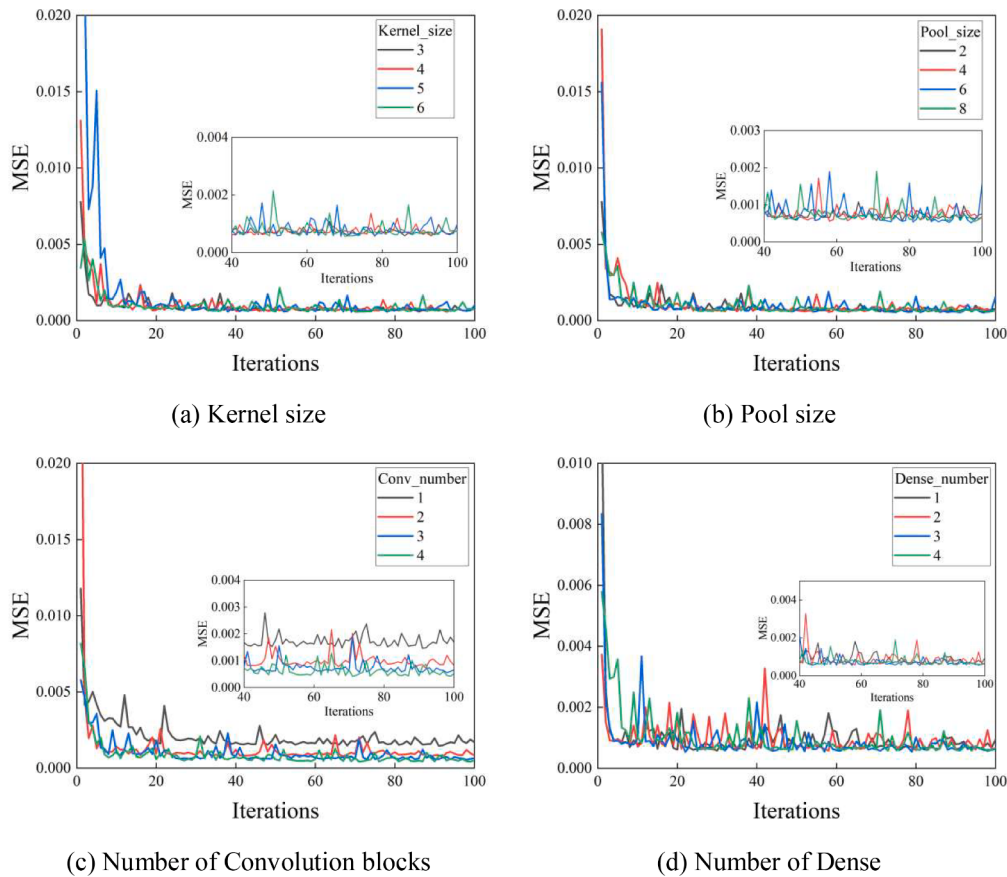


Fig. 20. Training process with different convolutional neural network parameters.

pooling layers, avoiding the constraints of manual feature design in extracting corrosion feature information.

5.2. Comparison between traditional methods and neural network methods

Fig. 23 and Table 9 display the results of calculations conducted on three experimental samples (IDTS 2, IDTS 3, IDTS 4) along with some

Table 8
Network structure of CNN-image.

Network layer	Value	Input size	Output size
Conv layer	Kernel_size=3, Kernel_number=32, Padding=same, Activation function=relu	90 × 90 × 1	90 × 90 × 32
Conv layer	Kernel_size=3, Kernel_number=32, Padding=same, Activation function=relu	90 × 90 × 32	90 × 90 × 32
Pooling layer	Pool_size=2, Stride=2, Padding=same	90 × 90 × 32	45 × 45 × 32
Conv layer	Kernel_size=3, Kernel_number=64, Padding=same, Activation function=relu	45 × 45 × 32	45 × 45 × 64
Conv layer	Kernel_size=3, Kernel_number=64, Padding=same, Activation function=relu	45 × 45 × 64	45 × 45 × 64
Pooling layer	Pool_size=2, Stride=2, Padding=same	45 × 45 × 64	23 × 23 × 64
Conv layer	Kernel_size=3, Kernel_number=128, Padding=same, Activation function=relu	23 × 23 × 64	23 × 23 × 128
Conv layer	Kernel_size=3, Kernel_number=128, Padding=same, Activation function=relu	23 × 23 × 128	23 × 23 × 128
Pooling layer	Pool_size=2, Stride=2, Padding=same	23 × 23 × 128	12 × 12 × 128
Flatten		12 × 12 × 128	18432
Fully Connected Layer	Neurons=64, Activation function=LeakyReLU, Dropout rate=0.5	18432	64
Fully Connected Layer	Neurons=32, Activation function=LeakyReLU, Dropout rate=0.5	64	32
Fully Connected Layer	Neurons=8	32	8
Fully Connected Layer	Neurons=1	8	1

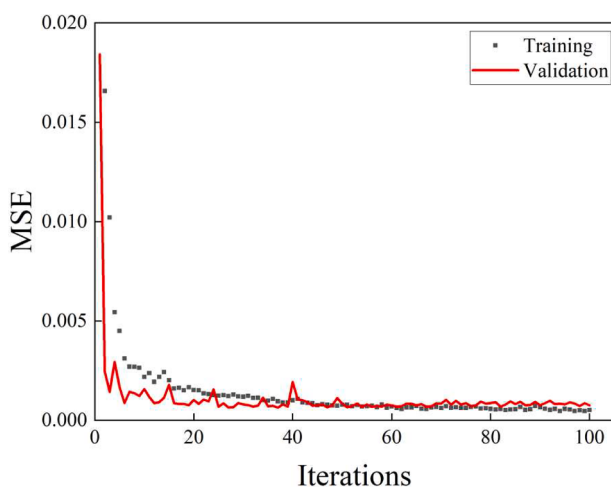


Fig. 21. Training result of the CNN-image.

test set samples using various methods (* denotes neural network-based methods proposed in this paper, # denotes methods in standard codes, + denotes modified methods suggested by other scholars [27,49]). The

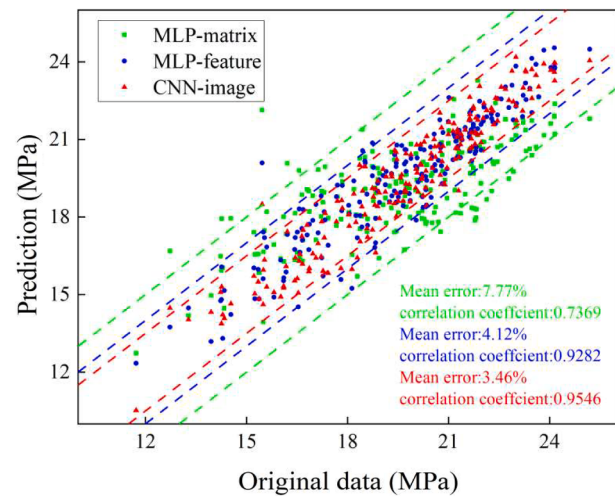


Fig. 22. Comparison of test results for three neural network-based methods.

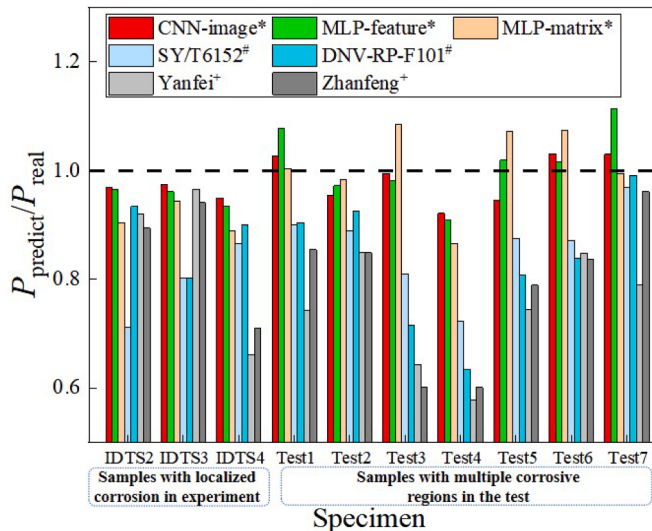


Fig. 23. Calculation results of different evaluation methods.

experimental samples represent pipes with localized corrosion, while the test samples represent pipes with multiple corrosive regions.

On the one hand, existing standards for corroded pipelines tend to be conservative in evaluating remaining strength, with average and maximum errors of 16.08% and 36%, respectively. On the other hand, traditional modified methods deliver reliable predictive performance when evaluating experimental samples containing small-area corrosion; however, they perform less effectively compared to standard codes when assessing complex-shaped samples of the test dataset, resulting in an average error of 23%. In contrast, the average errors for the CNN-image, MLP-feature, and MLP-matrix methods are 3.59%, 4.21%, and 7.32%, respectively, with the CNN-image method achieving a maximum error of only 4.52%. These prediction results align closely with the actual results.

Generally, standard methods provide concise evaluation approaches based on theoretical analysis and experimental data. However, due to their conservative nature, these methods are only suitable for the initial evaluation of corroded pipelines. Traditional modified methods primarily focus on higher-order fitting of multiple corrosion parameters in small corrosion regions, inevitably leading to overfitting issues. They still exhibit significant limitations in the overall evaluation of corroded pipelines. In contrast, neural network-based methods, especially CNN-

Table 9
Errors of various methods (%).

Specimen		CNN-image*	MLP-feature*	MLP-matrix*	SY#	DNV#	Yanf ⁺	Zhanf ⁺
Exp.	Avg	3.74	4.31	6.88	14.63	16.47	25.04	20.96
	Max	4.52	11.47	15.93	27.83	36.57	42.30	39.95
Test	Avg	2.87	3.65	7.32	24.30	13.16	21.81	18.84
	Max	3.13	3.90	13.45	28.84	19.76	42.3	39.95

image, apply to various corrosion scenarios and can offer valuable insights to develop remaining strength evaluation methods for corroded pipelines.

6. Conclusions

This study introduces an efficient method for establishing a pipe model with multiple corrosive regions, aligning more closely with actual corrosion morphology. Based on this method, the study creates a dataset of 3,000 samples and extracts corrosion information from these models using digital images. Then, three neural network evaluation frameworks are constructed: MLP-matrix, MLP-feature, and CNN-image. The study examines the relationship between various corrosion features and the failure pressure, optimizes the training parameters of the three network models, and compares the evaluation performance of the methods. Finally, the study contrasts the results of various methods with samples in the experiment and the test dataset, confirming the feasibility and advancement of neural network-based methods.

- (1) Utilizing the overall corrosion matrix extracts corrosion information, significantly enhancing modeling efficiency. For pipeline models with multiple corrosive regions, the proposed approach reduces the average creation time to just several minutes, providing a viable alternative to the previously required hours or days for such tasks.
- (2) Parameters associated with defect depth are the most critical factors influencing failure pressure, but individual corrosion features alone cannot decisively determine the outcome. Among the numerous corrosion features extracted, depth-related parameters strongly correlate with failure pressure. In addition, the stability and effectiveness of neural network training significantly decrease without depth-related features.
- (3) Adjusting parameters or methods can effectively enhance the training performance of neural networks. For instance, employing regularization methods to address overfitting and using data augmentation to increase the diversity and quantity of data improves the model's generalization capability and robustness.
- (4) Among the three neural network methods, the CNN-image method demonstrates the best predictive performance due to its high extraction of corrosion feature information. The average errors and correlation coefficients for MLP-matrix, MLP-feature, and CNN-image are 7.77%, 4.12%, 3.46%, and 0.7369, 0.9282, 0.9546, respectively.
- (5) Compared to results obtained from various methods on experimental and the test set dataset, neural network-based methods demonstrate high computational accuracy and applicability to a wide range of corrosion scenarios. These results indicate that the methods can provide valuable insights for further developing remaining strength evaluation methods for corroded pipelines.
- (6) The core focus of this study is on the parent material at the center of pipe joints, which presents a higher susceptibility to corrosion in welded parts and can be a key area for future research.

Nomenclature

(continued)

L_0	Length of pipeline
t	Thickness of pipeline
d_{\max}	Maximum depth of corrosion
W_{\max}	Maximum width of corrosion
S	Area of the corrosion defects
S_0	Area of the pipe
d_{75}	The 75th percentile depth of corrosion
ν	Poisson ratio
D	The diameter of the outer pipeline
E	Elastic modulus
L_{\max}	Maximum length of corrosion
V	The volume of the corrosion defects
V_0	The volume of the pipe
d_{50}	The 50th percentile depth of corrosion

CRediT authorship contribution statement

Zhiwei Zhang: Writing – review & editing, Writing – original draft, Visualization, Methodology, Investigation, Conceptualization. **Songling Li:** Writing – review & editing, Visualization, Validation, Supervision, Resources, Project administration, Methodology, Conceptualization. **Huajie Wang:** Validation, Supervision, Funding acquisition, Conceptualization. **Hongliang Qian:** Visualization, Validation, Conceptualization. **Changqing Gong:** Visualization, Validation, Conceptualization. **Qiongyao Wu:** Visualization, Validation, Conceptualization. **Feng Fan:** Project administration, Conceptualization.

Declaration of competing interest

The authors declare that they have no known competing financial interests or personal relationships that could have appeared to influence the work reported in this paper.

Data availability

No data was used for the research described in the article.

Acknowledgments

This work was financially supported by the National Key Research and Development Program of China (Grant No. 2023YFC3805601), National Natural Science Foundation of China (Grant No. 52308161), and the Shandong Provincial Natural Science Foundation (Grant No. ZR2023QE279 and ZR2023ME215).

References

- [1] Jin Z, Zhao X, Zhao T, Li J. Chloride ions transportation behavior and binding capacity of concrete exposed to different marine corrosion zones. Constr Build Mater 2018;177:170–83. <https://doi.org/10.1016/j.conbuildmat.2018.05.120>.
- [2] Akbari H, Pooyarad A. Wave force on protected submarine pipelines over porous and impermeable beds using SPH numerical model. Appl Ocean Res 2020;98. <https://doi.org/10.1016/j.apor.2020.102118>.
- [3] Amaya-Gómez R, Sánchez-Silva M, Muñoz F, Schoefs F, Bastidas-Arteaga E. Spatial characterization and simulation of new defects in corroded pipeline based on In-Line Inspections. Reliab Eng Syst Saf 2024;241:109697. <https://doi.org/10.1016/j.ress.2023.109697>.
- [4] Woldesellasse H, Tesfamariam S, Woldesellasse H, Tesfamariam S. Consequence assessment of gas pipeline failure caused by external pitting corrosion using an integrated Bayesian belief network and GIS model: application with Alberta

- pipeline. Reliab Eng Syst Saf 2023;240:109573. <https://doi.org/10.1016/j.ress.2023.109573>.
- [5] Eastvedt D, Naterer G, Duan X. Detection of faults in subsea pipelines by flow monitoring with regression supervised machine learning. Process Saf Environ Prot 2022;161:409–20. <https://doi.org/10.1016/j.psep.2022.03.049>.
- [6] Group EGPIP. 5–9th reports of the European gas pipeline incident data group (Period 1970–2013). Amsterdam, The Netherlands: European Gas Pipeline Incident Data Group; 2015.
- [7] ASME. B31G: manual for determining the remaining strength of corroded pipelines: a supplement to ANSI/ASME B31 code for pressure piping. American Society of Mechanical Engineers; 1991.
- [8] Batte A, Fu B, Kirkwood M, Vu D. New methods for determining the remaining strength of corroded pipelines. In: Proceedings of the international conference on offshore mechanics and arctic engineering. American Society of Mechanical Engineers; 1997. p. 221–8.
- [9] ASME. B31G: manual for determining the remaining strength of corroded pipelines: a supplement to ASME B31 code for pressure piping. American Society of Mechanical Engineers; 2012.
- [10] CSA C. Z662-07: limit state equation for burst of large leaks and rupture for corrosion defect, oil and gas pipeline systems. Mississauga: Canadian Standards Association; 2007.
- [11] Stephens DR, Leis BN. Development of an alternative criterion for residual strength of corrosion defects in moderate- to high-toughness pipe. In: Proceedings of the 3rd international pipeline conference; 2000.
- [12] DNV G. DNV-RP-F101 corroded pipelines recommended practice. Oslo, Norway: GCS AS; 2017.
- [13] SY/T6151. Corrosion damage evaluation methods for steel pipeline bodies. Bei Jing, China: National Energy Administration of China; 2009.
- [14] Ma B, Shuai J, Liu D, Xu K. Assessment on failure pressure of high strength pipeline with corrosion defects. Eng Fail Anal 2013;32:209–19. <https://doi.org/10.1016/j.engfailanal.2013.03.015>.
- [15] Amaya-Gomez R, Sanchez-Silva M, Bastidas-Arteaga E, Schoefs F, Munoz F. Reliability assessments of corroded pipelines based on internal pressure—a review. Eng Fail Anal 2019;98:190–214. <https://doi.org/10.1016/j.engfailanal.2019.01.064>.
- [16] Benjamin AC, Freire JL, Vieira RD, Cunha DJS. Interaction of corrosion defects in pipelines—Part 1: fundamentals. Int J Press Vessels Pip 2016;144:56–62. <https://doi.org/10.1016/j.ijpvp.2016.05.007>.
- [17] Teixeira AP, Palencia OG, Guedes Soares C. Reliability analysis of pipelines with local corrosion defects under external pressure. J Offshore Mech Arct Eng Trans ASME 2019;141. <https://doi.org/10.1115/1.4042384>.
- [18] de Souza RD, Benjamin AC, Freire JL, Vieira RD, Diniz JLC. Burst tests on pipeline containing long real corrosion defects. In: Proceedings of the international pipeline conference; 2004. p. 1159–67.
- [19] Bhardwaj U, Teixeira AP, Soares CG. Failure assessment of corroded ultra-high strength pipelines under combined axial tensile loads and internal pressure. Ocean Eng 2022;257. <https://doi.org/10.1016/j.oceaneng.2022.111438>.
- [20] Choi JB, Goo BK, Kim JC, Kim YJ, Kim WS. Development of limit load solutions for corroded gas pipelines. Int J Press Vessels Pip 2003;80:121–8. [https://doi.org/10.1016/s0308-0161\(03\)00005-x](https://doi.org/10.1016/s0308-0161(03)00005-x).
- [21] Bhardwaj U, Teixeira AP, Soares CG, Azad MS, Punurai W, Asavadorndeja P. Reliability assessment of thick high strength pipelines with corrosion defects. Int J Press Vessels Pip 2019;177. <https://doi.org/10.1016/j.ijpvp.2019.103982>.
- [22] Chen Y, Zhang H, Zhang J, Liu X, Li X, Zhou J. Failure assessment of X80 pipeline with interacting corrosion defects. Eng Fail Anal 2015;47:67–76. <https://doi.org/10.1016/j.engfailanal.2014.09.013>.
- [23] Mondal BC, Dhar AS. Interaction of multiple corrosion defects on burst pressure of pipelines. Can J Civ Eng 2017;44:589–97. <https://doi.org/10.1139/cjce-2016-0602>.
- [24] Sun J, Cheng YF. Modelling of mechano-electrochemical interaction of multiple longitudinally aligned corrosion defects on oil/gas pipelines. Eng Struct 2019;190:9–19. <https://doi.org/10.1016/j.engstruct.2019.04.010>.
- [25] Sun J, Cheng YF. Investigation by numerical modeling of the mechano-electrochemical interaction of circumferentially aligned corrosion defects on pipelines. Thin-Walled Struct 2019;144. <https://doi.org/10.1016/j.tws.2019.106314>.
- [26] Zhou R, Gu X, Luo X. Residual strength prediction of X80 steel pipelines containing group corrosion defects. Ocean Eng. 2023;274. <https://doi.org/10.1016/j.oceaneng.2023.114077>.
- [27] Chen Y, Zhang H, Zhang J, Li X, Zhou J. Failure analysis of high strength pipeline with single and multiple corrosions. Mater Des 2015;67:552–7. <https://doi.org/10.1016/j.matdes.2014.10.088>.
- [28] Amandi KU, Diennuodeke EO, Briggs TA. Model for remaining strength estimation of a corroded pipeline with interacting defects for oil and gas operations. Cogent Eng 2019;6. <https://doi.org/10.1080/23311916.2019.1663682>.
- [29] Zhang S, Zhou W. Assessment of effects of idealized defect shape and width on the burst capacity of corroded pipelines. Thin-Walled Struct 2020;154:106806. <https://doi.org/10.1016/j.tws.2020.106806>.
- [30] Li S, Zhang Z, Qian H, Wang H, Fan F. Research on remaining bearing capacity evaluation method for corroded pipelines with complex shaped defects. Ocean Eng 2024;296:116805. <https://doi.org/10.1016/j.oceaneng.2024.116805>.
- [31] Mokhtari M, Melchers RE. A new approach to assess the remaining strength of corroded steel pipes. Eng Fail Anal 2018;93:144–56. <https://doi.org/10.1016/j.engfailanal.2018.07.011>.
- [32] Mahmood W, Mohammed AS, Asteris PG, Ahmed H. Soft computing techniques to predict the early-age compressive strength of flowable ordinary Portland cement. Soft Comput 2023;27:3133–50. <https://doi.org/10.1007/s00500-022-07505-x>.
- [33] Hai-Bang L, Binh Thai P, Lu Minh L, Tien-Thinh L, Vuong Minh L, Asteris PG. Estimation of axial load-carrying capacity of concrete-filled steel tubes using surrogate models. Neural Comput Appl 2021;33:3437–58. <https://doi.org/10.1007/s00521-020-05214-w>.
- [34] Silva RCC, Guerreiro JNC, Loula AFD. A study of pipe interacting corrosion defects using the FEM and neural networks. Adv Eng Softw 2007;38:868–75. <https://doi.org/10.1016/j.advengsoft.2006.08.047>.
- [35] Phan HC, Dhar AS. Predicting pipeline burst pressures with machine learning models. Int J Press Vessels Pip 2021;191. <https://doi.org/10.1016/j.ijpvp.2021.104384>.
- [36] Le TT. Practical machine learning-based prediction model for axial capacity of square CFST columns. Mech Adv Mater Struct 2022;29:1782–97. <https://doi.org/10.1080/15376494.2020.1839608>.
- [37] Xiao R, Zayed T, Meguid MA, Sushama L. Improving failure modeling for gas transmission pipelines: a survival analysis and machine learning integrated approach. Reliab Eng Syst Saf 2024;241:109672. <https://doi.org/10.1016/j.ress.2023.109672>.
- [38] Zhang T, Shuai J, Shuai Y, Hua L, Xu K, Xie D, et al. Efficient prediction method of triple failure pressure for corroded pipelines under complex loads based on a backpropagation neural network. Reliab Eng Syst Saf 2023;231:108990. <https://doi.org/10.1016/j.ress.2022.108990>.
- [39] Mazumder RK, Salman AM, Li Y. Failure risk analysis of pipelines using data-driven machine learning algorithms. Struct Saf 2021;89. <https://doi.org/10.1016/j.strusafe.2020.102047>.
- [40] Abyani M, Bahaa MR, Zarrin M, Nasseri M. Predicting failure pressure of the corroded offshore pipelines using an efficient finite element based algorithm and machine learning techniques. Ocean Eng 2022;254. <https://doi.org/10.1016/j.oceaneng.2022.111382>.
- [41] Wang Y, Xia M, Su C. Multi-objective maintenance strategy for corroded pipelines considering the correlation of different failure modes. Reliab Eng Syst Saf 2024; 243:109894. <https://doi.org/10.1016/j.ress.2023.109894>.
- [42] Marques Ferreira AD, Afonso SMB, Willmersdorf RB, Lyra PRM. Multiresolution analysis and deep learning for corroded pipeline failure assessment. Adv Eng Softw 2021;162–3. <https://doi.org/10.1016/j.advengsoft.2021.103066>.
- [43] Li X, Jia R, Zhang R. A data-driven methodology for predicting residual strength of subsea pipeline with double corrosion defects. Ocean Eng 2023;279. <https://doi.org/10.1016/j.oceaneng.2023.114530>.
- [44] Hieu Chi P, Tien-Thinh L, Nang Duc B, Huan Thanh D, Tiep Duc P. An empirical model for bending capacity of defected pipe combined with axial load. Int J Press Vessels Pip 2021;191. <https://doi.org/10.1016/j.ijpvp.2021.104368>.
- [45] Lu H, Iseley T, Matthews J, Liao W, Azimi M. An ensemble model based on relevance vector machine and multi-objective salp swarm algorithm for predicting burst pressure of corroded pipelines. J Pet Sci Eng 2021;203. <https://doi.org/10.1016/j.petrol.2021.108585>.
- [46] Soomro AA, Mokhtar AA, Kurnia JC, Lashari N, Lu H, Sambo C. Integrity assessment of corroded oil and gas pipelines using machine learning: a systematic review. Eng Fail Anal 2022;131. <https://doi.org/10.1016/j.engfailanal.2021.105810>.
- [47] Su Y, Li J, Yu B, Zhao Y, Yao J. Fast and accurate prediction of failure pressure of oil and gas defective pipelines using the deep learning model. Reliab Eng Syst Saf 2021;216. <https://doi.org/10.1016/j.ress.2021.108016>.
- [48] Oh D, Race J, Oterkun S, Koo B. Burst pressure prediction of API 5L X-grade dented pipelines using deep neural network. J Mar Sci Eng 2020;8. <https://doi.org/10.3390/jmse8100766>.
- [49] Jiang F, Dong S. Probabilistic-based burst failure mechanism analysis and risk assessment of pipelines with random non-uniform corrosion defects, considering the interacting effects. Reliab Eng Syst Saf 2024;242:109783. <https://doi.org/10.1016/j.ress.2023.109783>.
- [50] Miao X, Zhao H. Corroded submarine pipeline degradation prediction based on theory-guided IMOSOA-EL model. Reliab Eng Syst Saf 2024;243:109902. <https://doi.org/10.1016/j.ress.2023.109902>.
- [51] Miao X, Zhao H, Gao B, Song F. Corrosion leakage risk diagnosis of oil and gas pipelines based on semi-supervised domain generalization model. Reliab Eng Syst Saf 2023;238:109486. <https://doi.org/10.1016/j.ress.2023.109486>.
- [52] Ma Y, Zheng J, Liang Y, Klemes JJ, Du J, Liao Q, et al. Deeppipe: theory-guided neural network method for predicting burst pressure of corroded pipelines. Process Saf Environ Prot 2022;162:595–609. <https://doi.org/10.1016/j.psep.2022.04.036>.
- [53] Yang Y, Khan F, Thodi P, Abbassi R. Corrosion induced failure analysis of subsea pipelines. Reliab Eng Syst Saf 2017;159:214–22. <https://doi.org/10.1016/j.ress.2016.11.014>.
- [54] Chen ZF, Li X, Sang Z, Wang W, Wang Y. A novel dynamic parameter method (DPM) based on ANN for safety assessment of corroded pipelines. Ocean Eng 2023; 280. <https://doi.org/10.1016/j.oceaneng.2023.114922>.
- [55] Chen ZF, Chu WP, Wang HJ, Li Y, Wang W, Meng WM, et al. Structural integrity assessment of hydrogen-mixed natural gas pipelines based on a new multi-parameter failure criterion. Ocean Eng 2022;247. <https://doi.org/10.1016/j.oceaneng.2022.110731>.
- [56] Ma H, Wang H, Geng M, Ai Y, Zhang W, Zheng W. A new hybrid approach model for predicting burst pressure of corroded pipelines of gas and oil. Eng Fail Anal 2023;149. <https://doi.org/10.1016/j.engfailanal.2023.107248>.
- [57] Brockhaus S, Ginten M, Klein S, Teckert M, Stawicki O, Oevermann D, et al. 10-In-line inspection (ILI) methods for detecting corrosion in underground pipelines.

- editor. In: Orazem ME, editor. *Underground pipeline corrosion*. Woodhead Publishing; 2014. p. 255–85.
- [58] Hopkins P. 3-Assessing the significance of corrosion in onshore oil and gas pipelines. editor. In: Orazem ME, editor. *Underground pipeline corrosion*. Woodhead Publishing; 2014. p. 62–84.
- [59] Zhang Z, Wang H, Qian H, Feng Q, Jin X, Fan F. Comparative analysis and applicability of corrosion test methods for construction steel components. *Case Stud Constr Mater* 2023;18. <https://doi.org/10.1016/j.cscm.2023.e02034>.
- [60] Amaya-Gómez R, Schoefs F, Sánchez-Silva M, Muñoz F, Bastidas-Arteaga E. Matching of corroded defects in onshore pipelines based on In-Line Inspections and Voronoi partitions. *Reliab Eng Syst Saf* 2022;223:108520. <https://doi.org/10.1016/j.ress.2022.108520>.
- [61] Benjamin AC, Freire JLF, Vieira RD, Diniz JLC, de Andrade EQ. Burst tests on pipeline containing interacting corrosion defects. In: Proceedings of the 24th international conference on offshore mechanics and arctic engineering. ASME; 2005. p. 403–17.
- [62] Skelton R, Maier HJ, Christ HJ. The Bauschinger effect, Masing model and the Ramberg–Osgood relation for cyclic deformation in metals. *Mater Sci Eng A Struct Mater Prop Microstruct Process* 1997;238:377–90.
- [63] Freire JLF, Vieira RD, Castro JTP, Benjamin AC. Part 5: rupture tests of pipeline containing complex-shaped metal loss defects. *Exp Tech* 2010;31:57–62.
- [64] Patil S, Karuppanan S, Kuppusamy S, et al. Buckling strength of corroded pipelines with interacting corrosion defects: numerical analysis. *Int J Struct Stab Dyn* 2016; 16.
- [65] Benjamin AC, Franzoi AR, Freire JLF, Vieira RD, Diniz JLC. Burst tests on pipeline containing irregular shaped corrosion defects. IPC; 2008.
- [66] Zhang Z, Gao Y, Wang H, Qian H, Chen H, Jin X, et al. A sub-region-based method for evaluating regularly and irregularly corroded steel tubes under axial compression. *Structures* 2023;54:556–69. <https://doi.org/10.1016/j.struc.2023.05.041>.
- [67] Iannaccone L, Sharma N, Tabandeh A, Gardoni P. Modeling time-varying reliability and resilience of deteriorating infrastructure. *Reliab Eng Syst Saf* 2022;217. <https://doi.org/10.1016/j.ress.2021.108074>.
- [68] Iannaccone L, Gardoni P. Physics-based repair rate curves for segmented pipelines subject to seismic excitations. *Sustain Resilient Infrastruct* 2023;8:121–41. <https://doi.org/10.1080/23789689.2021.2000146>.
- [69] Wang H, Zhang Z, Qian H, Fan F. Effect of local corrosion on the axial compression behavior of circular steel tubes. *Eng Struct*. 2020;224. <https://doi.org/10.1016/j.engstruct.2020.111205>.
- [70] Cosham A, Hopkins P, Macdonald KA. Best practice for the assessment of defects in pipelines-corrosion. *Eng Fail Anal* 2007;14:1245–65. <https://doi.org/10.1016/j.enganfailanal.2006.11.035>.
- [71] Iannaccone L, Gardoni P. Time-varying fragility functions for bridges subject to main shock-aftershock sequences including damage accumulation during the events and calibration based on available data. In: Proceedings of the 10th international conference on bridge maintenance, safety and management (IABMAS); 2021. p. 2787–94. Electr Network.
- [72] Pluvinage G, Bouledroua O, Meliani MH, Suleiman R. Corrosion defect analysis using domain failure assessment diagram. *Int J Press Vessels Pip* 2018;165:126–34. <https://doi.org/10.1016/j.ijpvp.2018.06.005>.
- [73] Shuai J, Bu W. Statistical analysis of pipeline operating parameters and inspection data. *Oil Gas Storage Transp* 2006. 35-7+2.
- [74] Srivastava N, Hinton G, Krizhevsky A, Sutskever I, Salakhutdinov R. Dropout: a simple way to prevent neural networks from overfitting. *J Mach Learn Res* 2014; 15:1929–58.
- [75] Hoerl A, Kennard R. Ridge regression: biased estimation for nonorthogonal problems. *Technometrics* 2000;42(1):7.
- [76] Krizhevsky A, Sutskever I, Hinton G. ImageNet classification with deep convolutional neural networks. *Adv Neural Inf Process Syst* 2012;25.
- [77] Simonyan K, Zisserman A. Very deep convolutional networks for large-scale image recognition. *Comput Sci* 2014.